Progress In Electromagnetics Research B, Vol. 81, 163–182, 2018

Quad-Band Wearable Slot Antenna with Low SAR Values for 1.8 GHz DCS, 2.4 GHz WLAN and 3.6/5.5 GHz WiMAX Applications

Danvir Mandal[1, *] and Shyam S. Pattnaik[2]

Abstract—In this paper, a quad-band wearable slot antenna with low specific absorption rate (SAR) is presented. By cutting an inverted V-shaped slot with its arms further extended towards the center of the circular patch, multiple resonant modes of the antenna can be excited to operate on 1.8 GHz DCS, 2.4 GHz WLAN and 3.6/5.5 GHz WiMAX bands. The measured peak gains and impedance bandwidths are about 4.91/7.84/2.58/4.12 dBi and 320/60/80/180 MHz for the 1.8/2.4/3.6/5.5 GHz bands respectively. The SAR of the proposed antenna has been measured using a three layer human tissue model. The estimated SAR values at all the resonant frequencies are well below the threshold limit of 2 W/kg, which ensures its viability for wearable applications. In order to approximate different parts of the human body, the SAR values have been estimated for three surface sizes, $120 \times 120\,\text{mm}^2$, $220 \times 220\,\text{mm}^2$ and $320 \times 320\,\text{mm}^2$, of the human tissue model, and results are compared. Frequency detuning of the proposed antenna due to bending along x, y and x-y planes has also been carried out and discussed. Further, on arm effect on the antenna performance is investigated, and results are presented. The simulated and measured results are in good agreement, which validates the use of proposed wearable antenna in DCS/WLAN/WiMAX bands.

1. INTRODUCTION

In recent days, due to advent of wearable sensors and body centric communication systems, it is desirable to integrate many wireless communication standards in a single wireless device for personal wireless communication. In order to satisfy these communication standards, wearable multiband antennas which can operate at 1.7–1.9 GHz for Digital Cellular System (DCS), 2.4–2.484 GHz/5.15–5.825 GHz for Wireless Local Area Network (WLAN) and 3.4–3.69 GHz/5.25–5.85 GHz for Worldwide Interoperability for Microwave Access (WiMAX) are required.

Many multiband slot antennas have been proposed in the past few years [1–7]. In [1], dual band operation has been achieved in polygon shaped wearable patch antenna with circular slot and vertical slits on a jeans substrate. Triple band antennas proposed by using U shaped, C and inverted L shaped slots have been reported in [2] and [3]. A triple band switchable antenna with three sickle shaped slots in ground plane is reported in [4]. Further compact triple band slot antennas with microstrip and square slots have been presented in [5] and [6]. The Four band characteristics of the slot antenna reported in [7] were generated by etching rectangular slot and inverted T and E shaped stubs. A multiband antenna for LTE/GSM/UMTS and a multi-slot antenna for wireless body arear network have been reported in [8] and [9].

For wearable antennas, SAR value is a vital parameter. Many human tissue models have been used in past for the calculation of SAR. Low SAR antennas have been presented in [10–12]. Human body

Received 25 May 2018, Accepted 10 July 2018, Scheduled 19 July 2018
* Corresponding author: Danvir Mandal (danvir.mandal@gmail.com).
[1] I. K. Gujral Punjab Technical University, Kapurthala, Punjab 144603, India. [2] National Institute of Technical Teachers Training and Research, Chandigarh 160026, India.

effects on implantable antennas for single equivalent layer and three layer human tissue models have been presented in [13]. The electromagnetic energy absorption by homogeneous and layered human tissue models has been analyzed in [14] and [15]. In [16], layered cubic and cylindrical human tissue models have been used for SAR calculations. The bending and on arm effect on a wearable antenna has been analyzed in [17] and [18].

A circular patch antenna primarily supports TM^z modes where z is perpendicular to the patch. In order to find the modes of a circular patch antenna, the circular patch, ground plane, and the substrate between the two are considered as a circular cavity [19].

In this work, a quad-band wearable slot antenna with a circular patch has been designed on polyester substrate [17]. The antenna has low SAR values at all the resonating frequencies, making it viable for wearable applications. Apart from SAR, bending is another major factor that affects the antenna performance. The effect of bending on frequency detuning of the proposed antenna has also been measured and discussed along x, y and x-y planes. Finally, on arm effect, with and without cloth, have been analyzed and results are presented.

The antenna structure and design procedure are explained in Section 2. In Section 3, the results of the simulated and handmade antennas are compared and discussed. This section also includes the SAR calculations, effect of bending and on arm performance of the antenna. The conclusions are drawn in Section 4.

2. ANTENNA STRUCTURE AND DESIGN

The basic structure of the proposed quad-band wearable slot antenna is illustrated in Figure 1. Copper tape is used for preparing circular patch and square ground plane.

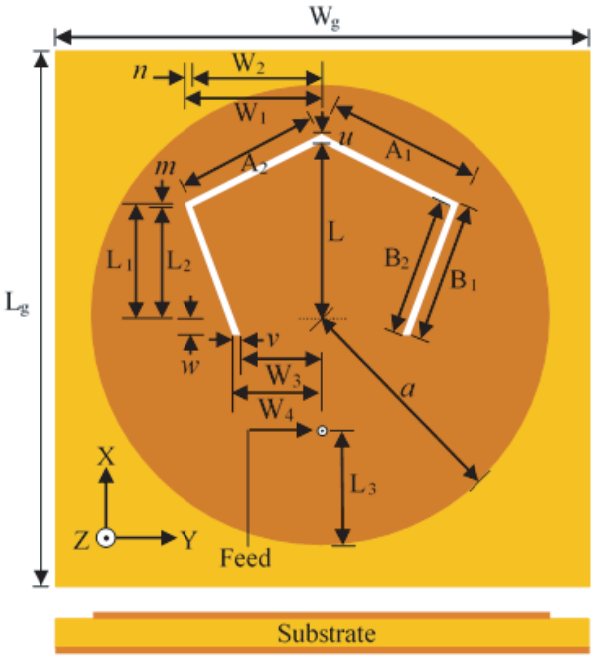

Figure 1. Quad-band wearable slot antenna.

A polyester cloth substrate with thickness, $h = 2.0\,\text{mm}$, dielectric constant, $\varepsilon_r = 1.39$, and loss tangent, $\tan\delta = 0.01$ is used to design and fabricate the proposed antenna. The size of the fabricated antenna considering the ground plane size is $70 \times 70\,\text{mm}^2$. At first, the radius a of the circular patch is calculated using standard expression given in [19]. The first four modes of circular patch antenna are TM^z_{110}, TM^z_{210}, TM^z_{010}, and TM^z_{310}. The dominant mode is the TM^z_{110}, whose resonant frequency is

given by

$$(f_r)_{110} = \frac{1.8412\, v_0}{2\pi a\sqrt{\epsilon_r}} \tag{1}$$

where v_0 is the speed of light in free-space.

The radius a of the circular patch is corrected by taking fringing into account and the effective radius a_e is given by

$$a_e = a\left\{1 + \frac{2h}{\pi a\epsilon_r}\left[\ln\left(\frac{\pi a}{2h}\right) + 1.7726\right]\right\}^{1/2} \tag{2}$$

Therefore, the resonant frequency for the dominant mode TM^z_{110} is modified using Eq. (2) and given as

$$(f_r)_{110} = \frac{1.8412\, v_0}{2\pi a_e\sqrt{\epsilon_r}} \tag{3}$$

Considering resonant frequency, $f_r = 2.4$ GHz for TM^z_{110} mode, a is obtained approximately as 29.01 mm. The step by step design procedure is given as follows. Initially, a circular patch with $a = 30$ mm, $L_g = 70$ mm, $W_g = 70$ mm and $L_3 = 15.0$ mm is designed. This wearable circular patch antenna is designated Antenna I. After this, an inverted V-shaped slot is cut in the circular patch. For convenience, this circular patch with inverted V-shaped slot is designated Antenna II.

Finally, the arms of the inverted V-shaped slot are extended on both sides with slanted slots towards center of the patch. This final patch is designated Antenna III. The step by step design methodology and prototype of the handmade antenna is shown in Figure 2. The surface current distributions of circular patch with final slot at 1.8 GHz, 2.4 GHz, 3.6 GHz and 5.5 GHz are shown in Figures 3 to 6.

The current density distribution for 1.8 GHz shows that the current distribution is dense, inside and around the slot, whereas for 2.4 GHz band, current distribution is dense, only inside the slot. However,

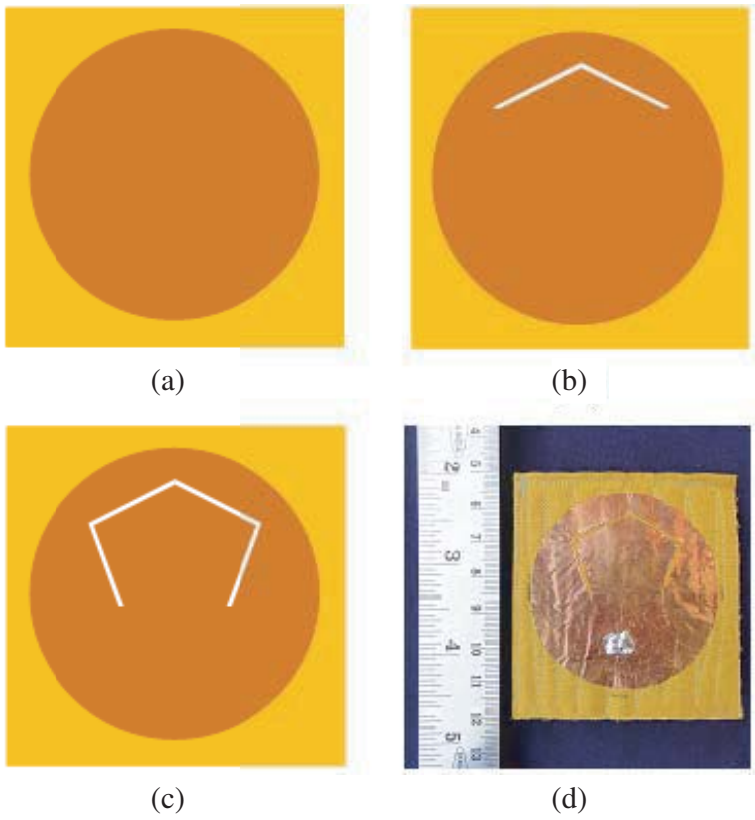

Figure 2. Geometries of (a) Antenna I, (b) Antenna II with inverted V-shaped slot, (c) Antenna III with final slot, (d) photograph of handmade Antenna III.

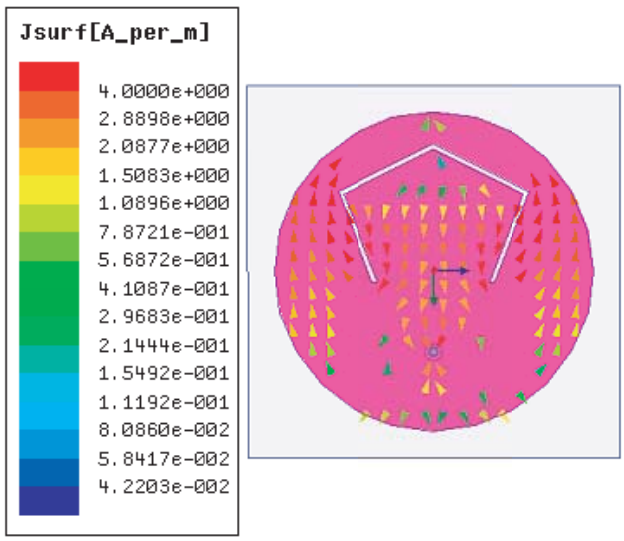

Figure 3. Surface current distribution of Antenna III at 1.8 GHz.

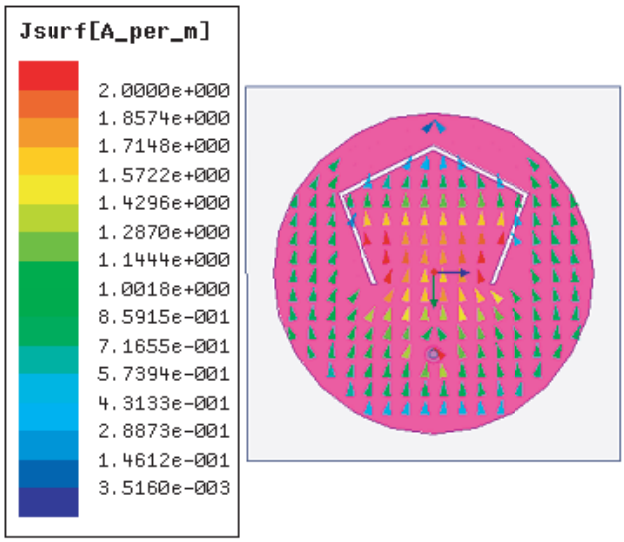

Figure 4. Surface current distribution of Antenna III at 2.4 GHz.

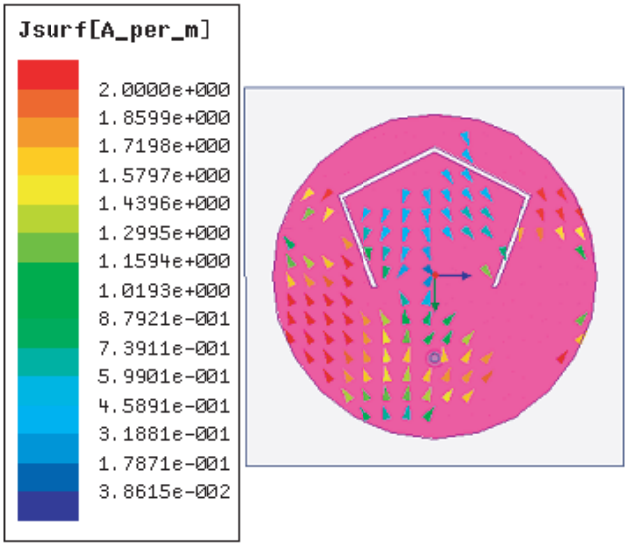

Figure 5. Surface current distribution of Antenna III at 3.6 GHz.

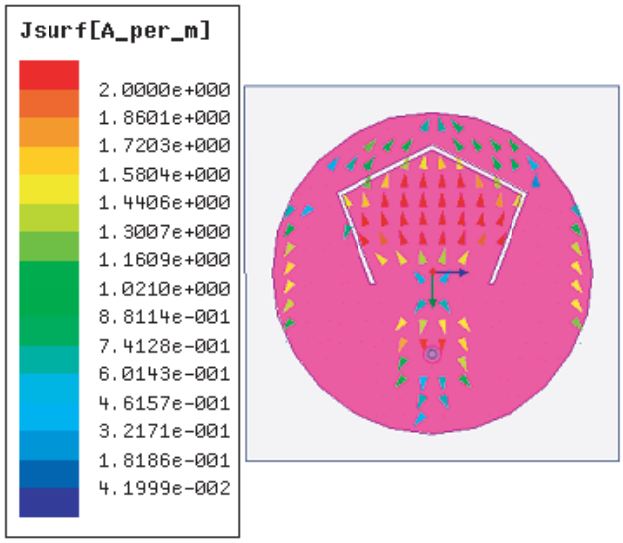

Figure 6. Surface current distribution of Antenna III at 5.5 GHz.

for 2.4 GHz, the current is flowing all over the circular patch. Similarly, the current distribution for 3.6 GHz is dense on the lower left side of the patch. For 5.5 GHz, dense current distribution is observed only inside the slot and sparse current distribution outside the slot.

The geometrical parameters used to fabricate the wearable quad-band antenna are listed in Table 1. The expressions derived for the estimation of A_1, A_2, B_1 and B_2 are given as

$$A_1 = \left(W_1^2+(L-L_1+u)^2\right)^{1/2} \tag{4}$$

$$A_2 = \left(W_2^2+(L-L_2)^2\right)^{1/2} \tag{5}$$

$$B_1 = \left((W_1-W_4)^2+(L_1+w)^2\right)^{1/2} \tag{6}$$

$$B_2 = \left((W_2 - W_3)^2 + (L_2 + w)^2\right)^{1/2} \quad (7)$$

Table 1. Parameters of the proposed low SAR quad-band wearable slot antenna.

Parameters (unit: mm)	Antenna II	Antenna III
L	23	23
L_1	15	15
L_2	14.5	14.5
W_1	18	18
W_2	17	17
A_1	20.12	20.12
A_2	19.0	19.0
m	0.5	0.5
n	1.0	1.0
u	1.0	1.0
B_1	-	18.20
B_2	-	17.73
W_3	-	11.5
W_4	-	10.5
v	-	1.0
w	-	2.0

3. RESULTS AND DISCUSSION

The antenna design is simulated using High Frequency Structure Simulator (HFSS). The fabricated antenna is tested using ANRITSU MS46322A vector network analyzer. The simulated and measured reflection coefficient (S_{11}) plots are shown in Figure 7 and Figure 8.

The obtained impedance bandwidths are given in Table 2. Antenna I cover two bands from 2.33 GHz to 2.44 GHz and 3.95 GHz to 4.01 GHz. Antenna II has four bands that cover from 2.12 GHz to 2.21 GHz, 3.12 GHz to 3.16 GHz, 4.03 GHz to 4.04 GHz and 5.43 GHz to 5.62 GHz. Antenna III satisfies the requirement of DCS, WLAN and WiMAX applications. Antenna III covers four bands from 1.70 GHz to 2.01 GHz, 2.39 GHz to 2.50 GHz, 3.59 GHz to 3.70 GHz and 5.41 GHz to 5.65 GHz with impedance bandwidths of 310 MHz, 110 MHz, 110 MHz and 240 MHz respectively. The simulated resonant frequencies of the Antenna III are 1.88 GHz, 2.44 GHz, 3.64 GHz and 5.54 GHz.

Table 2. Simulated and measured impedance bandwidths (%) for the proposed low SAR quad-band wearable slot antenna.

Antenna	Band I (GHz) /BW (%)	Band II (GHz) /BW (%)	Band III (GHz) /BW (%)	Band IV (GHz) /BW (%)
Antenna I	2.33–2.44/4.6	3.95–4.01/1.5	-	-
Antenna II	2.12–2.21/4.2	3.12–3.16/1.3	4.03–4.04/0.2	5.43–5.62/3.4
Antenna III	1.70–2.01/16.7	2.39–2.50/4.5	3.59–3.70/3.0	5.41–5.65/4.3
Antenna III (Measured)	1.64–1.96/17.7	2.37–2.43/2.5	3.55–3.63/2.2	5.39–5.57/3.3

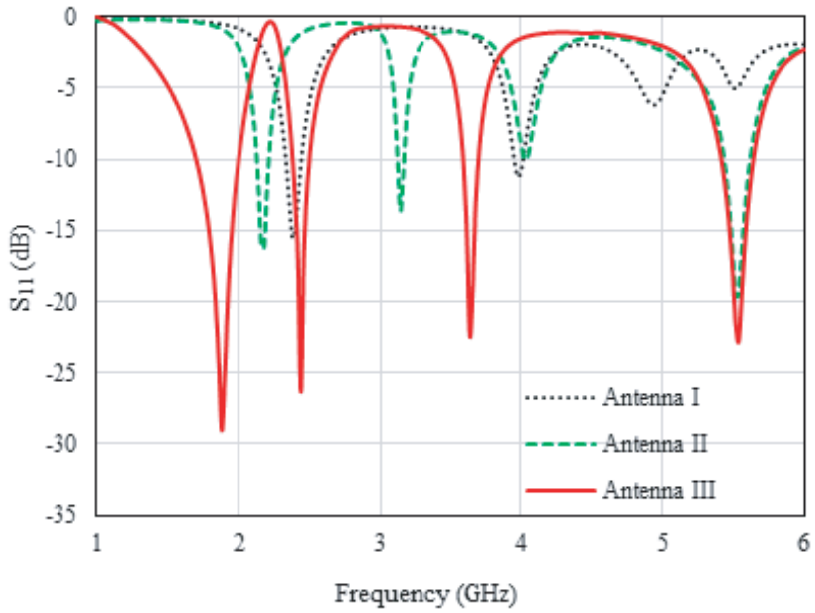

Figure 7. Simulated reflection coefficient (S_{11}) of Antenna I, Antenna II and Antenna III.

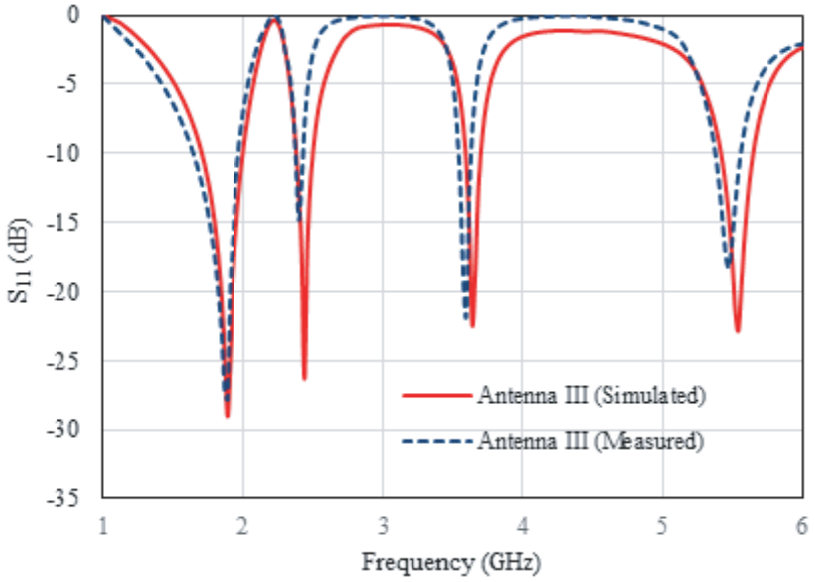

Figure 8. Simulated and measured reflection coefficient (S_{11}) of Antenna III.

The measured operating bands of Antenna III range in 1.64–1.96 GHz, 2.37–2.43 GHz, 3.55–3.63 GHz and 5.39–5.57 GHz with the impedance bandwidth of 320 MHz, 60 MHz, 80 MHz and 180 MHz respectively. The measured resonant frequencies of the Antenna III are 1.88 MHz, 2.4 GHz, 3.6 GHz and 5.48 GHz.

The simulated and measured radiation patterns at center frequencies of the four bands, i.e., 1.8 GHz, 2.4 GHz, 3.6 GHz and 5.5 GHz, can be observed in Figure 9 to Figure 12. Figure 13 shows the measured peak gain of the proposed handmade Antenna III. The Inset in Figure 13 shows the photograph of the quad band wearable antenna in anechoic chamber during gain and radiation pattern measurement.

The gain of the proposed antenna is measured using the following expression:

$$\text{Gain of the Test Antenna} = G + (P_T - P_R) \tag{8}$$

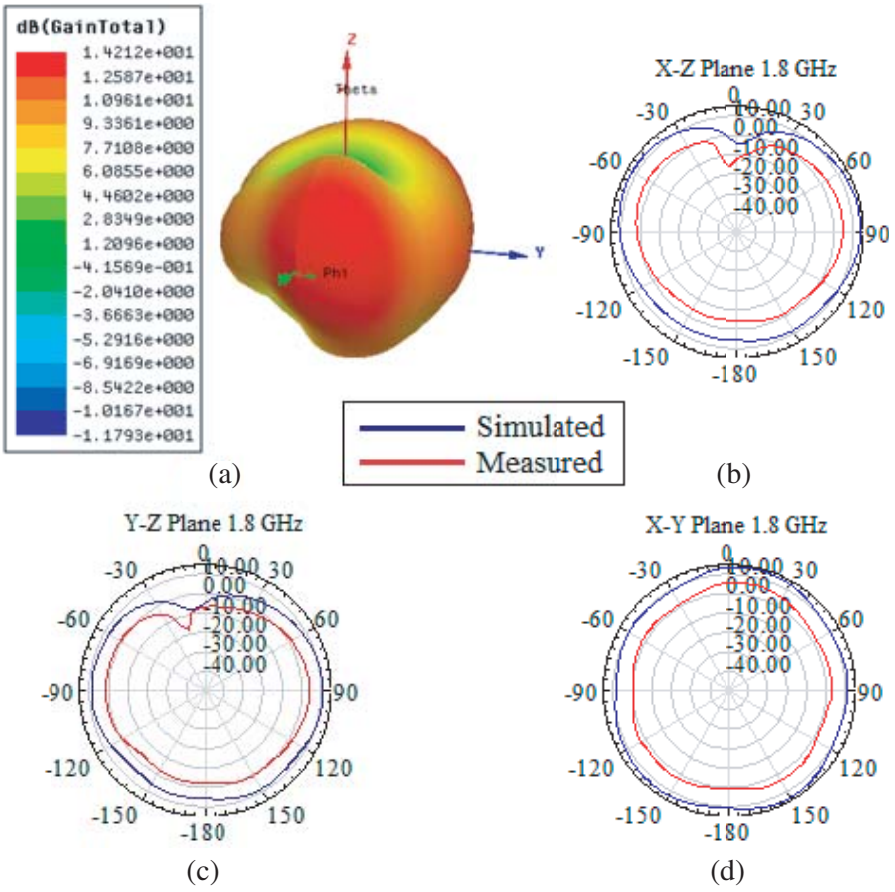

Figure 9. (a) 3-D simulated radiation pattern at 1.8 GHz, 2-D simulated and measured radiation patterns at 1.8 GHz, (b) X-Z plane, (c) Y-Z plane, (d) X-Y plane.

Table 3. Material parameters of human tissue layers.

Tissue Layer	Frequency (GHz)	Permittivity (ε_r)	Conductivity σ (S/m)
Skin	1.8	38.87	1.184
	2.4	38.06	1.440
	3.6	36.92	2.085
	5.5	35.36	3.463
Fat	1.8	5.349	0.078
	2.4	5.285	0.102
	3.6	5.164	0.160
	5.5	4.982	0.273
Muscle	1.8	54.44	1.389
	2.4	53.63	1.774
	3.6	52.05	2.768
	5.5	49.42	4.832

where G is the gain of the reference pyramidal horn antenna known over anisotropic antenna, P_T the power received by test antenna, and P_R the power received by reference antenna. The measured peak gain of the proposed antenna at 1.8 GHz, 2.4 GHz, 3.6 GHz and 5.5 GHz is 4.91 dBi, 7.84 dBi, 2.58 dBi and 4.12 dBi respectively.

3.1. SAR Calculations

The proposed antenna is simulated in the vicinity of a three layer human tissue model, as shown in Figure 14. The thickness of the three human tissue layers used, i.e., skin, fat and muscle, are 3 mm, 13 mm and 60 mm. The gap between the antenna and skin layer is 5 mm. The values of the permittivity (ε_r) and conductivity (σ) of the skin, fat and muscle are obtained from [20]. The loss tangent and density of the layers are kept same as of [1] and [15]. The material properties of human tissue layers used for SAR calculation are given in Table 3.

Initially, the surface size of $120 \times 120\,\text{mm}^2$ is considered for human tissue model. Further, to approximate different parts of the human body, the averaged SAR values are estimated for three ascending surface sizes of the human tissue model, i.e., $120\times120\,\text{mm}^2$, $220\times220\,\text{mm}^2$ and $320\times320\,\text{mm}^2$. The local SAR distributions at 1.8 GHz, 2.4 GHz, 3.6 GHz and 5.5 GHz, on the surface of the skin layer

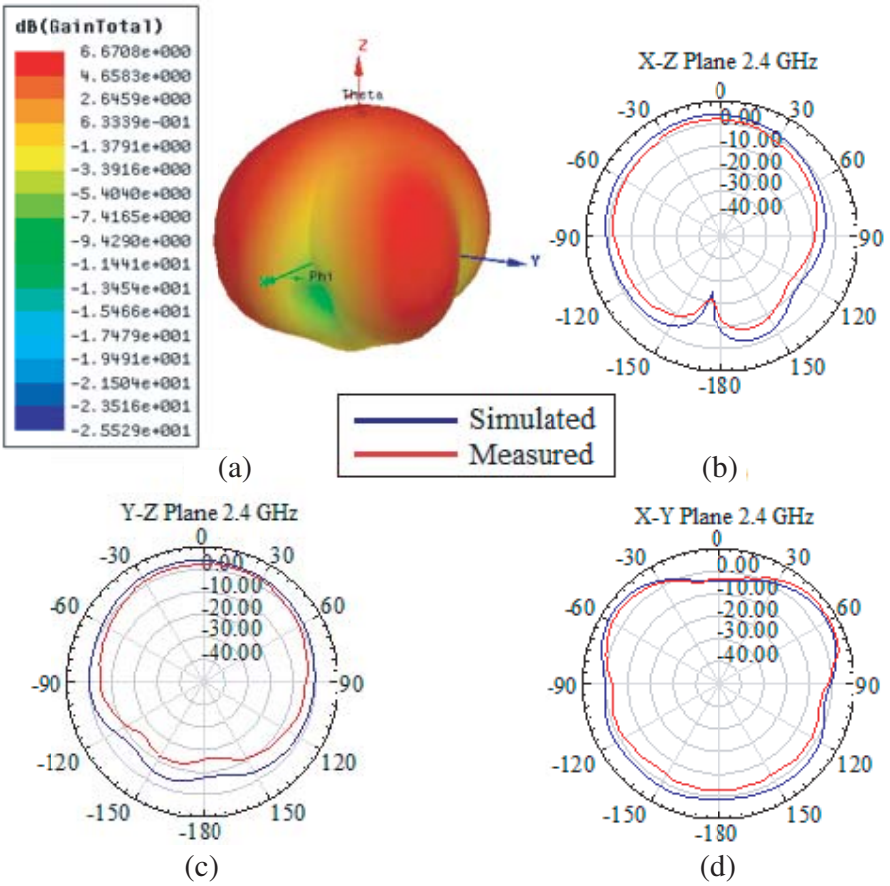

Figure 10. (a) 3-D simulated radiation pattern at 2.4 GHz, 2-D simulated and measured radiation patterns at 2.4 GHz, (b) X-Z plane, (c) Y-Z plane, (d) X-Y plane.

Table 4. Estimated SAR values for ascending surface sizes of the human tissue model.

Surface size (mm^2) of the human tissue model	Average SAR (W/kg)			
	1.8 GHz	2.4 GHz	3.6 GHz	5.5 GHz
120×120	0.121	0.411	0.874	0.954
220×220	0.048	0.394	0.791	0.881
320×320	0.019	0.358	0.566	0.798

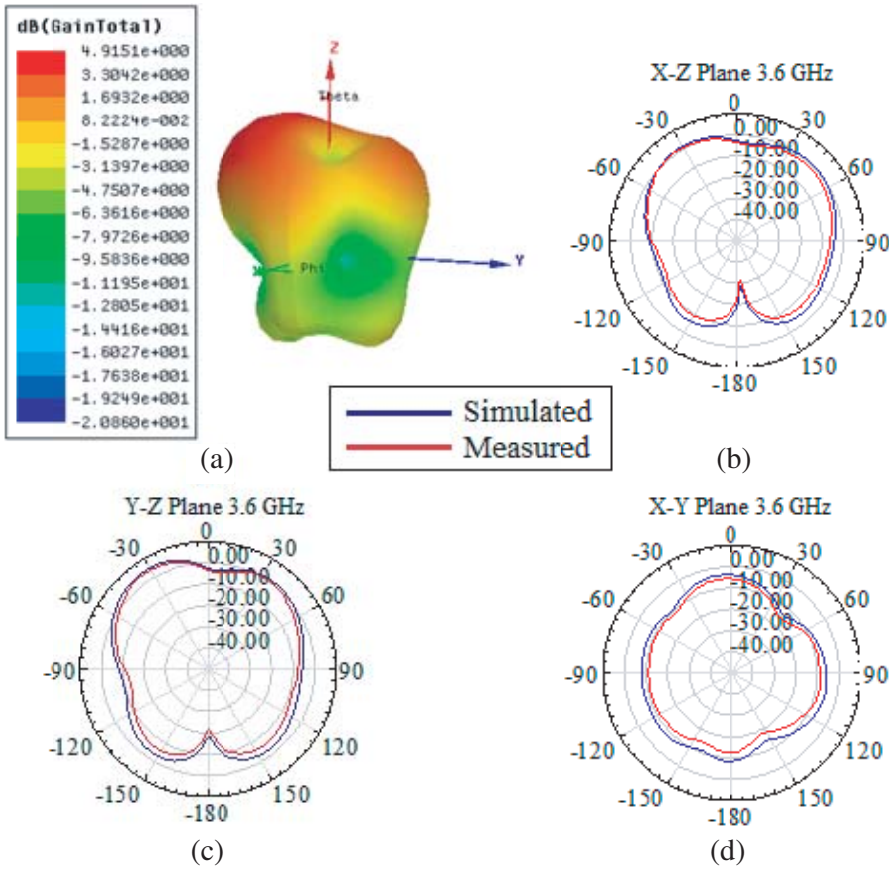

Figure 11. (a) 3-D simulated radiation pattern at 3.6 GHz, 2-D simulated and measured radiation patterns at 3.6 GHz, (b) X-Z plane, (c) Y-Z plane, (d) X-Y plane.

with 120×120 mm^2 surface size, are shown in Figures 15 to 18. The estimated SAR values of the proposed antenna for all resonant frequencies and surface sizes are summarized in Table 4. The simulations for SAR estimation are done in HFSS. The input power of 0.5 W is given to the antenna during SAR simulation. The averaged SAR is calculated using IEEE C95.3 standard, in which SAR is averaged over 10 g of biological tissue.

The maximum local SAR found in the skin layer of human tissue model at 1.8 GHz, 2.4 GHz, 3.6 GHz and 5.5 GHz is 0.274 W/kg, 1.065 W/kg, 2.137 W/kg and 2.374 W/kg respectively. The calculated averaged SAR values in human tissue model with 120×120 mm^2 surface size at 1.8 GHz, 2.4 GHz, 3.6 GHz and 5.5 GHz are 0.121 W/kg, 0.411 W/kg, 0.874 W/kg and 0.954 W/kg.

Similarly, the estimated averaged SAR values for 220×220 mm^2 and 320×320 mm^2 surface sizes at 1.8/2.4/3.6/5.5 GHz are 0.048/0.394/0.791/0.881 W/kg and 0.019/0.358/0.566/0.798 W/kg, respectively. It is observed that, with the increase in the surface size of the human tissue model, the averaged SAR values tend to decrease. The simulated radiation efficiency and maximum gain of the quad band wearable antenna in free space and over human tissue model (120×120 mm^2) are calculated and compared in Table 5. The simulated radiation efficiency of the proposed antenna at 1.8 GHz, 2.4 GHz, 3.6 GHz and 5.5 GHz in free space and over human tissue model is 92.45/75.22/63.26/88.95% and 85.11/68.07/44.29/77.65%, respectively.

The simulated maximum gain of the quad-band antenna in free space and over human tissue model at 1.8 GHz, 2.4 GHz, 3.6 GHz and 5.5 GHz is 14.21/6.67/4.91/6.70 dB and 13.10/6.63/3.76/6.11 dB respectively.

Figures 19 to 22, compare the simulated radiation patterns of the proposed antenna in free space with simulated radiation patterns over numerical human tissue model (120×120 mm^2). The simulated radiation patterns of the proposed antenna in free space and over human tissue model are quite different

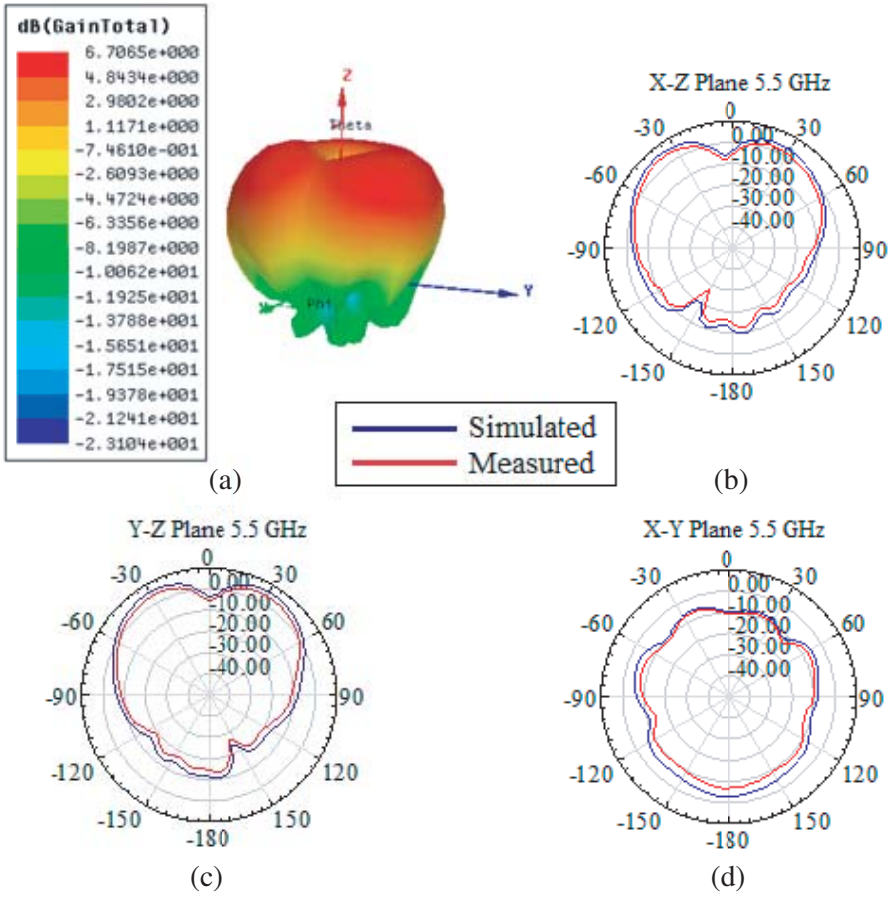

Figure 12. (a) 3-D simulated radiation pattern at 5.5 GHz, 2-D simulated and measured radiation patterns at 5.5 GHz, (b) X-Z plane, (c) Y-Z plane, (d) X-Y plane.

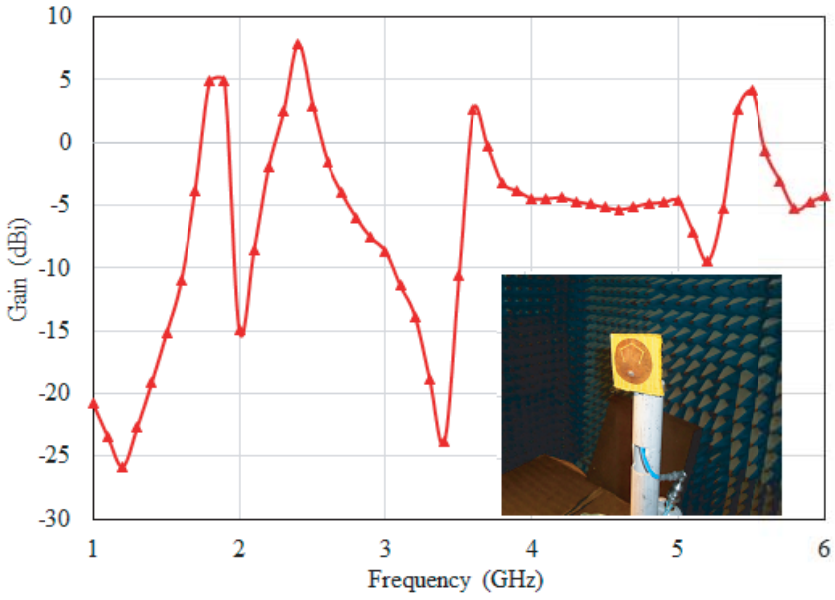

Figure 13. Measured peak gain of the proposed Antenna III.

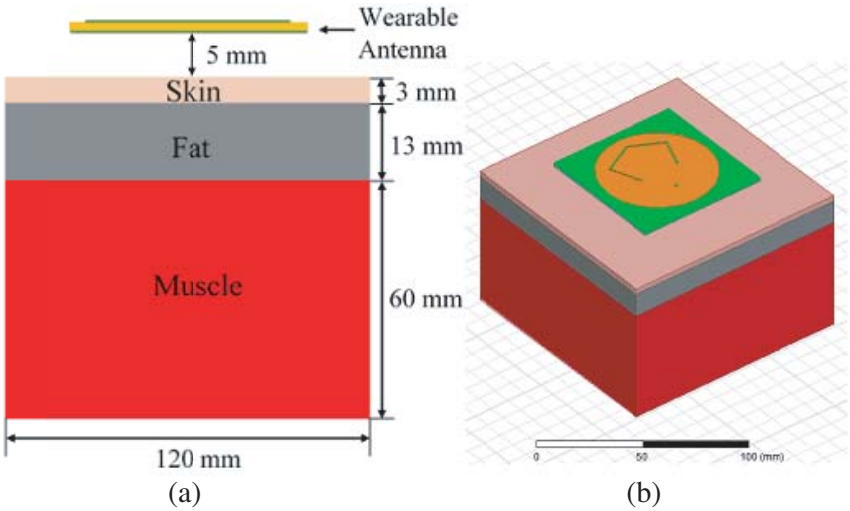

Figure 14. (a) Modelling of Antenna III on three layer human tissue for SAR estimation at 1.8 GHz, 2.4 GHz, 3.6 GHz and 5.5 GHz, (b) photograph of the proposed antenna over three layer human tissue model in HFSS.

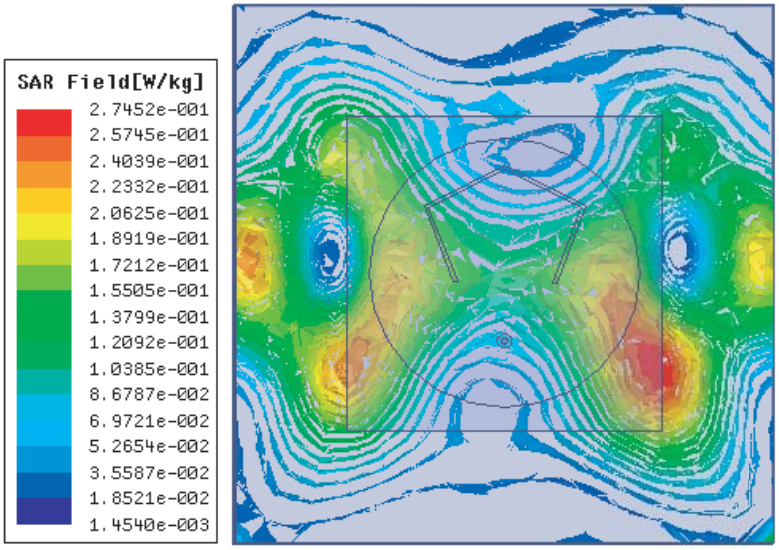

Figure 15. Local SAR distribution on the surface of skin layer at 1.8 GHz.

Table 5. Radiation efficiency and maximum gain in free space and over human tissue model.

Resonating Frequency	Radiation Efficiency (%)		Maximum Gain (dB)	
	In free space	Over human tissue model	In free space	Over human tissue model
1.8 GHz	92.45	85.11	14.21	13.10
2.4 GHz	75.22	68.07	6.67	6.63
3.6 GHz	63.26	44.29	4.91	3.76
5.5 GHz	88.95	77.65	6.70	6.11

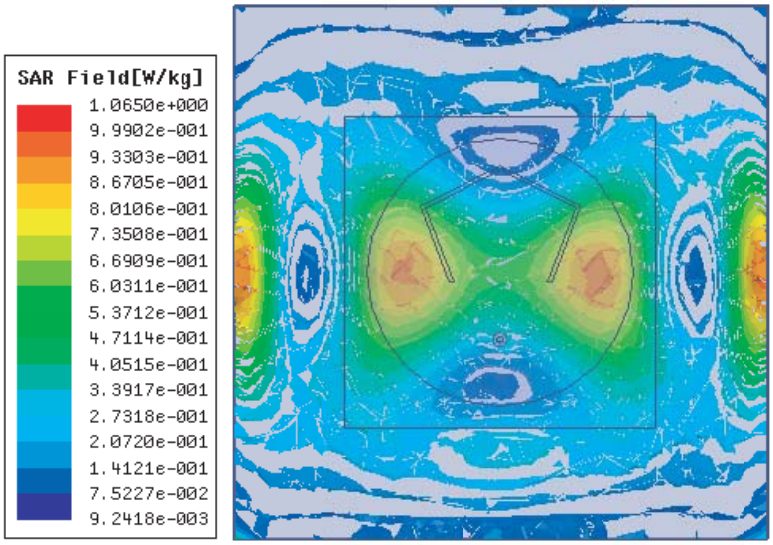

Figure 16. Local SAR distribution on the surface of skin layer at 2.4 GHz.

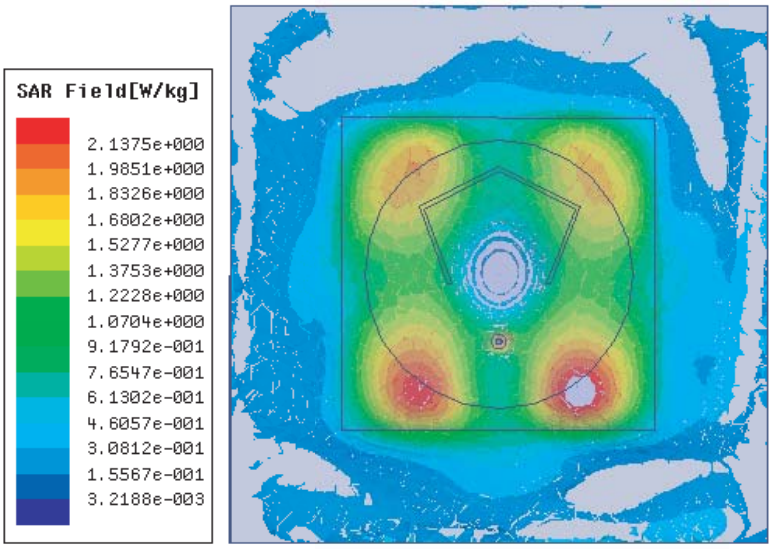

Figure 17. Local SAR distribution on the surface of skin layer at 3.6 GHz.

in X-Z and Y-Z planes, but in X-Y plane, the radiations patterns are almost similar at all the resonant frequencies.

3.2. Effect of Bending on Antenna Performance

The effect of bending is measured in x-plane, y-plane and x-y plane. The handmade prototype of Antenna III is bent by keeping it around a PVC (poly vinyl chloride) pipe as shown in Figure 23. The diameter of the PVC pipe is 150 mm. Figure 24 shows the measured reflection coefficient (S_{11}) of Antenna III under three bending conditions. The results show that lower frequency bands (1.8 GHz and 2.4 GHz) shifts to the left side of the spectrum with further decrease in reflection coefficient, when bent along x and y planes.

On the contrary, the higher frequency bands (3.6 GHz and 5.5 GHz) shift to the right side of the spectrum with decrease in reflection coefficient, when being bent along x and y planes. In x-

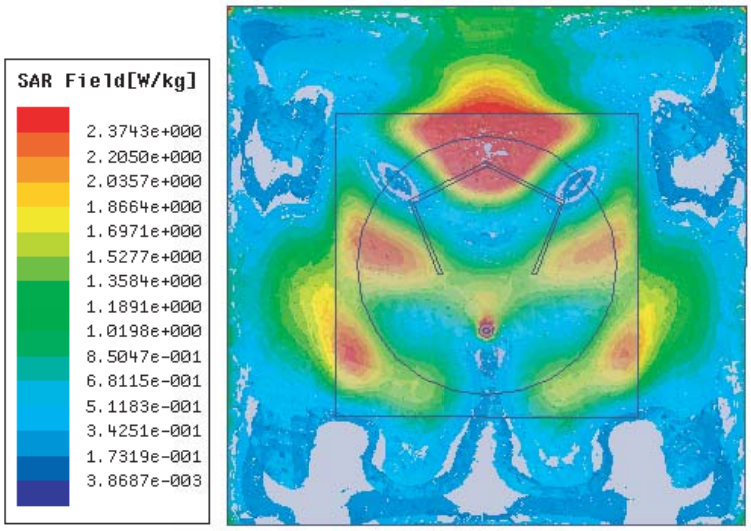

Figure 18. Local SAR distribution on the surface of skin layer at 5.5 GHz.

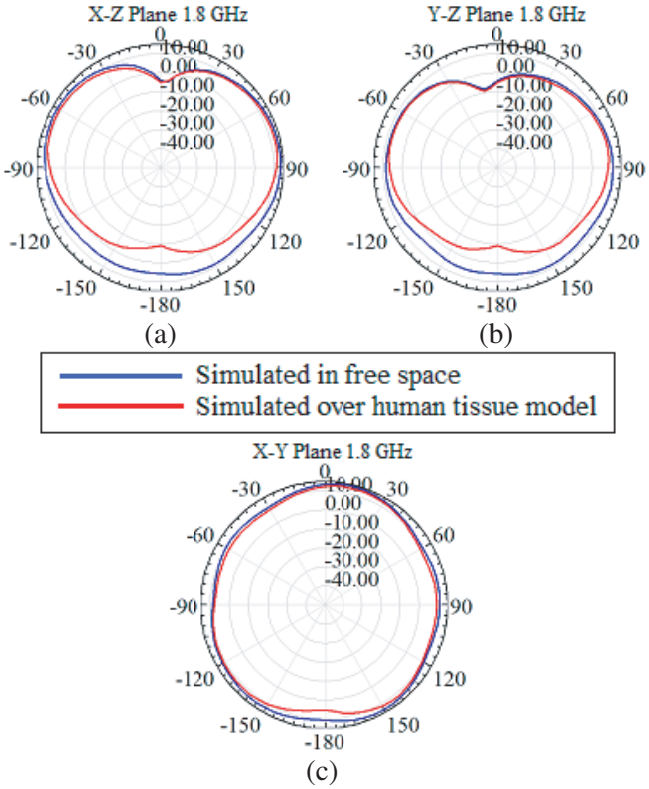

Figure 19. Comparison of 2-D simulated radiation patterns in free space and over human tissue model at 1.8 GHz. (a) X-Z plane, (b) Y-Z plane, (c) X-Y plane.

y plane bending, the lower bands and upper bands shift has landed approximately in between the lower bands and upper bands of x-plane and y-plane bending. Frequency detuning, which is observed when measurements are compared for all the three cases of bending is presented in Table 6. Maximum frequency detuning is observed for 1.8 GHz band when antenna is bent along x-plane, where as minimum frequency detuning is observed for 3.6 GHz band when antenna is bent along y-plane.

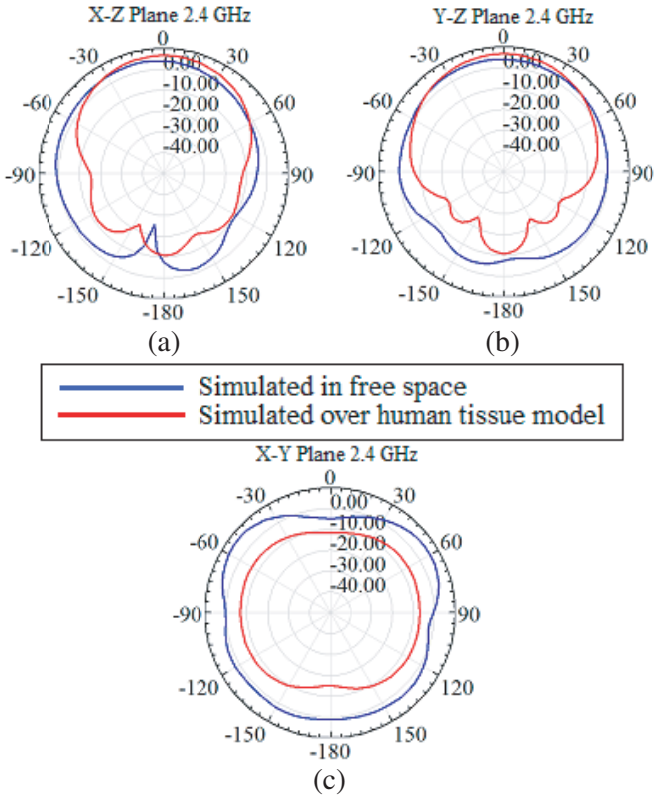

Figure 20. Comparison of 2-D simulated radiation patterns in free space and over human tissue model at 2.4 GHz. (a) X-Z plane, (b) Y-Z plane, (c) X-Y plane.

Table 6. Frequency detuning for bending in x, y and x-y plane.

Bending Case	Frequency detuning (%)			
	1.8 GHz Band	**2.4 GHz Band**	**3.6 GHz Band**	**5.5 GHz Band**
x-plane	7.45	6.67	3.34	4.01
y-plane	2.13	1.67	1.12	1.45
x-y plane	5.32	5.0	2.22	3.29

3.3. On Arm Effect on Antenna Performance

The on arm effect on antenna performance has also been analyzed. Four cases of the proposed antenna, on arm, are considered as shown in Figure 25. Two cases are x-plane and y-plane perpendicular to arm length, without cloth, and two cases are x-plane and y-plane perpendicular to arm length, with cloth.

Measured reflection coefficient of antenna on different arm conditions is shown in Figure 26. Frequency detuning, which is observed when measurements are compared for all the four cases of on arm performance are presented in Table 7. The 1.8 GHz band shifts to the left side of the spectrum for all four cases of on arm performance.

The 2.4 GHz band shifts to the left side for Case 1, does not shift for Case 2, and shifts to the right side of the spectrum for Cases 3 and 4 of on arm condition.

The 3.6 GHz band shifts to the left side for Case 1, shifts to the right side for Case 2, and shifts to the right side for Cases 3 and 4, respectively. The last 5.5 GHz band shifts to the left side for Cases 1 and 2, whereas it shifts to the right side of the spectrum for Cases 3 and 4. The maximum frequency detuning during on arm measurements is calculated at 1.8 GHz band for Cases 1 and 2. For 2.4 GHz

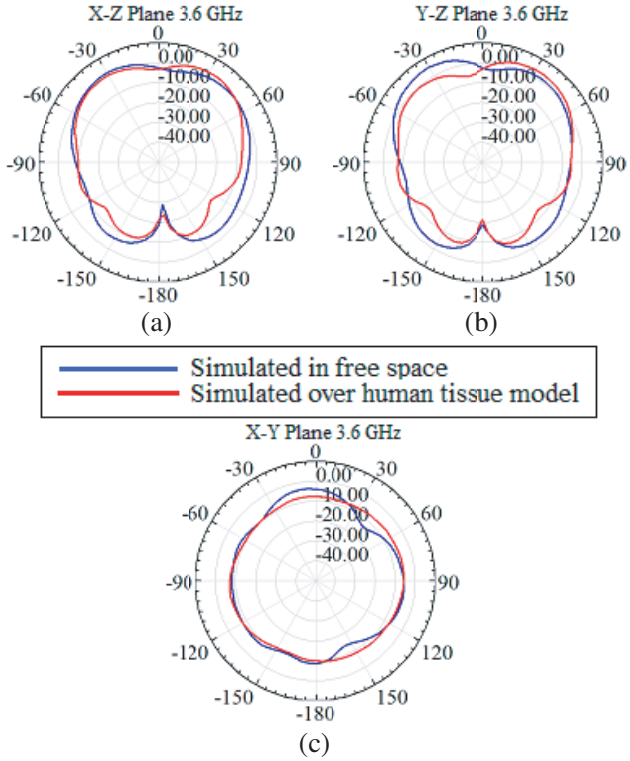

Figure 21. Comparison of 2-D simulated radiation patterns in free space and over human tissue model at 3.6 GHz. (a) X-Z plane, (b) Y-Z plane, (c) X-Y plane.

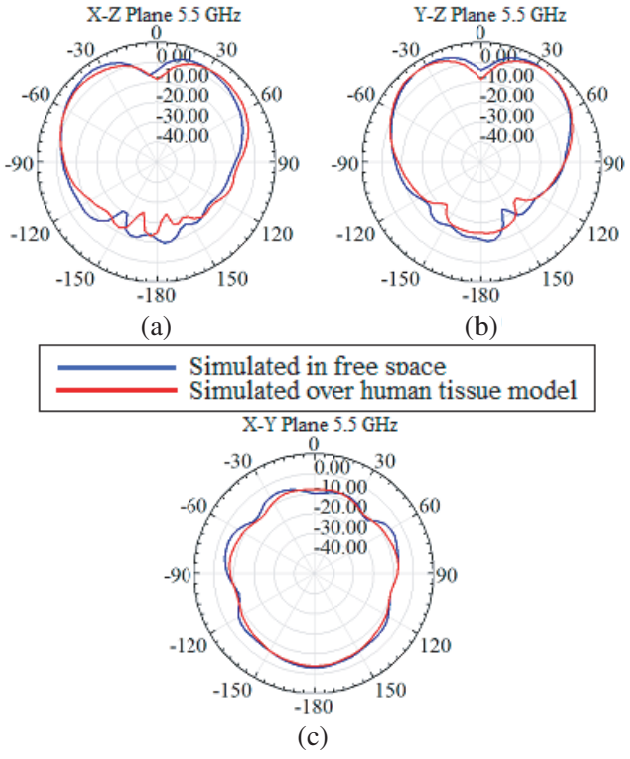

Figure 22. Comparison of 2-D simulated radiation patterns in free space and over human tissue model at 5.5 GHz. (a) X-Z plane, (b) Y-Z plane, (c) X-Y plane.

(a) (b) (c)

Figure 23. Photographs of quad-band wearable slot antenna under three bending conditions. (a) Bent along x-plane, (b) bent along y-plane, (c) diagonally bent along x-y plane.

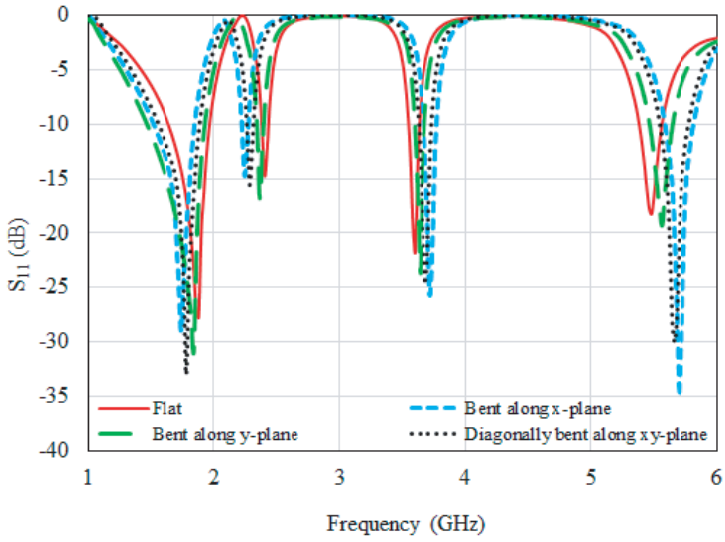

Figure 24. Reflection coefficient (S_{11}) characteristics of the quad-band wearable slot antenna under different bending conditions.

Table 7. Frequency detuning for different on arm conditions.

Case	On arm condition	Frequency detuning (%)			
		1.8 GHz Band	2.4 GHz Band	3.6 GHz Band	5.5 GHz Band
Case 1	x-plane perpendicular to arm length (w/o cloth)	9.58	1.67	1.11	1.09
Case 2	y-plane perpendicular to arm length (w/o cloth)	9.58	0.0	1.11	1.09
Case 3	x-plane perpendicular to arm length (with cloth)	2.13	4.17	5.0	1.46
Case 4	y-plane perpendicular to arm length (with cloth)	2.13	5.83	2.78	1.46

band, no shift in the frequency is observed for Case 2. Minimum frequency detuning has been found for Cases 1 and 2 at 5.5 GHz band.

Table 8 illustrates the comparison between the proposed antenna and the antennas described in the references. It can be seen that the dual band antenna in [1] has the smallest SAR value at 1.8 GHz, but its size is larger than that of our proposed antenna. The table reveals that the SAR values of the proposed antenna at all the resonant frequencies are lower than that of the other works listed in Table 8. The gain and radiation efficiency of the proposed antenna is better than almost all antennas proposed in references listed in Table 8. The antenna parameters which were not provided in references are marked with "x" in Table 8.

Table 8. Comparison of the proposed antenna with other published works.

Ref.	**Size (mm)**	**Resonant Frequency (GHz)**	**Bandwidth (MHz/%)**	**Gain (dBi)**	**Radiation Efficiency (%)**	**SAR (W/kg)**
[1]	240 ×240 ×1	0.9 1.8	x x	8.1 7.4	20.50 10.30	0.0011 0.0034
[8]	55 ×110 ×5	0.79–0.96 1.70–2.73	169 1030	−0.91–0.25 1.40–5.48	24–44 40–78	0.44 (0.84 GHz) 0.64 (0.935 GHz) 1.51 (1.85 GHz) 0.99 (2.45 GHz)
[9]	68.10 ×41.98 ×4.445	3.5 4.5 5.5	56.9 %	x x x	47 62 51	4.50 4.10 6.06
[10]	81 ×81 ×4	2.45	360	7.3	70	0.23
[11]	40 ×80 ×12	0.9 1.8	22 92	0.91 1.76	78.58 94.35	0.67 0.58
[12]	78 ×40 ×0.8	0.9 1.8 1.9 2.1	230.4 (0.725–0.95 GHz) 522.24 (1.74–2.25 GHz)	2.0 2.14 2.51 2.58	98 89 94 98	1.50 1.80 1.53 1.15
[14]	32 ×29 ×1.5	3.0 6.0 8.0	x x x	x x x	x x x	16.6 8.00 7.20
Proposed Antenna	70 ×70 ×2	1.8 2.4 3.6 5.5	320 60 80 180	4.91 7.84 2.58 4.12	92.45 75.22 63.26 88.95	0.019 0.358 0.566 0.798

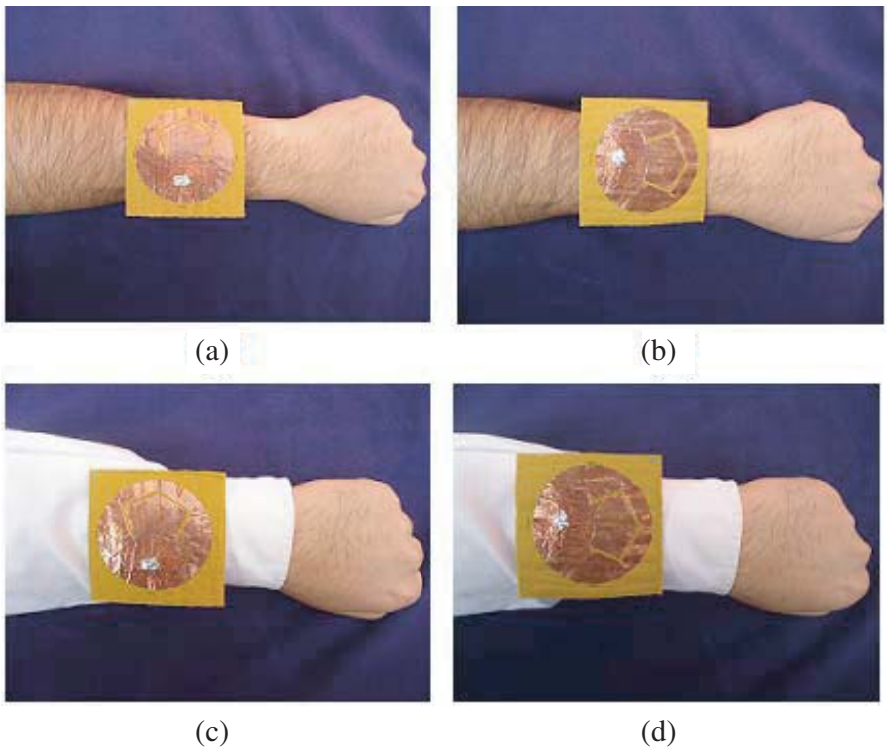

Figure 25. Photographs of quad-band wearable slot antenna on different arm conditions. (a) x-plane perpendicular to arm length (without cloth), (b) y-plane perpendicular to arm length (without cloth), (c) x-plane perpendicular to arm length (with cloth), (d) y-plane perpendicular to arm length (with cloth).

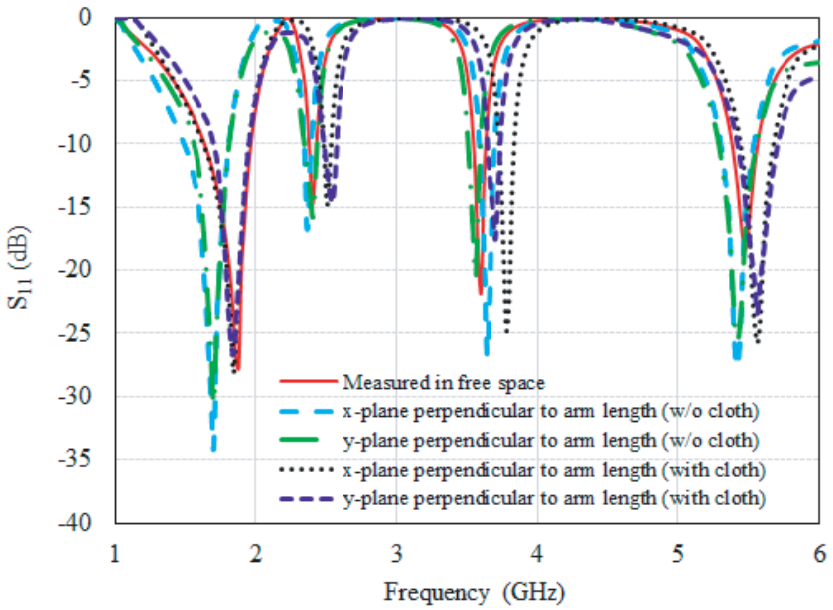

Figure 26. Reflection coefficient (S_{11}) characteristics of the quad-band wearable slot antenna on different arm conditions.

4. CONCLUSION

This paper presents a handmade low SAR quad-band wearable slot antenna and its design procedure, which is based on simple slot antenna design concepts. The antenna has shown appreciable gain and smooth radiation pattern characteristics over 1.8 GHz DCS, 2.4 GHz WLAN and 3.6/5.5 GHz WiMAX bands. The estimated SAR values at all the resonant frequencies lie well below the threshold limit of 2 W/kg, ensuring the feasibility of the proposed antenna for wearable applications. The results show that surface size of the human tissue model has significant effect on SAR calculations. With the increase in the surface size of the three layer human tissue model, the SAR values tend to decrease. This investigation offers selection criteria to choose the body part of the human body for antenna placement during SAR calculations. The effect of bending along x, y and x-y planes has also been investigated, and frequency detuning is presented and discussed. Finally, on arm performances of the proposed antenna, with cloth and without cloth, have been measured and discussed.

ACKNOWLEDGMENT

We acknowledge I. K. Gujral Punjab Technical University, Kapurthala, Punjab, India for providing the opportunity to do research and publish results.

REFERENCES

1. Sundarsingh, E. F., S. Velan, M. Kanagasabai, A. K. Sarma, C. Raviteja, and M. G. N. Alsath, "Polygon-shaped slotted dual-band antenna for wearable applications," *IEEE Antennas and Wireless Propagation Letters*, Vol. 13, 611–614, 2014.
2. Lee, K. F., S. L. S. Yang, and A. A. Kishk, "Dual- and multiband U-slot patch antennas," *IEEE Antennas and Wireless Propagation Letters*, Vol. 7, 645–647, 2008.
3. Lu, J. H. and B. J. Huang, "Planar compact slot antenna with multi-band operation for IEEE 802.16m application," *IEEE Transactions on Antennas and Propagation*, Vol. 61, No. 3, 1411–1414, Mar. 2013.
4. Saghati, A. P., M. Azarmanesh, and R. Zaker, "A novel switchable single- and multifrequency triple-slot antenna for 2.4-GHz bluetooth, 3.5-GHz WiMax, and 5.8-GHz WLAN," *IEEE Antennas and Wireless Propagation Letters*, Vol. 9, 534–537, 2010.
5. Dang, L., Z. Y. Lei, Y. J. Xie, G. L. Ning, and J. Fan, "A compact microstrip slot triple-band antenna for WLAN/WiMAX applications," *IEEE Antennas and Wireless Propagation Letters*, Vol. 9, 1178–1181, 2010.
6. Hu, W., Y. Z. Yin, P. Fei, and X. Yang, "Compact triband square-slot antenna with symmetrical L-strips for WLAN/WiMAX applications," *IEEE Antennas and Wireless Propagation Letters*, Vol. 10, 462–465, 2011.
7. Cao, Y. F., S. W. Cheung, and T. I. Yuk, "A multi-band slot antenna for GPS/WiMAX/WLAN systems," *IEEE Transactions on Antennas and Propagation*, Vol. 63, No. 3, 952–958, Mar. 2015.
8. Hong, Y., J. Tak, J. Baek, B. Myeong, and J. Choi, "Design of a multiband antenna for LTE/GSM/UMTS band operation," *International Journal of Antennas and Propagation*, Vol. 2014, Article ID 548160, 9 pages, 2014.
9. Wei, Y. F. and C. Roblin, "Multislot antenna with a screening backplane for UWB WBAN applications," *International Journal of Antennas and Propagation*, Vol. 2012, Article ID 731912, 12 pages, 2012.
10. Gao, G. P., B. Hu, S. F. Wang, and C. Yang, "Wearable circular ring slot antenna with EBG structure for wireless body area network," *IEEE Antennas and Wireless Propagation Letters*, Vol. 17, 434–437, 2018.
11. Kusuma, A. H., A. F. Sheta, I. Elshafiey, Z. Siddiqui, M. A. Alkanhal, S. Aldosari, and S. A. Alshebeili, "A new low SAR antenna structure for wireless handset applications," *Progress In Electromagnetic Research*, Vol. 112, 23–40, 2011.

12. Faruque, M. R. I., M. I. Hossain, and M. T. Islam, "Low specific absorption rate microstrip patch antenna for cellular phone applications," *IET Microwaves, Antennas & Propagation*, Vol. 9, No. 14, 1540–1546, 2015.
13. Gemio, J., J. Parron, and J. Soler, "Human body effects on implantable antennas for ISM bands applications: Models comparison and propagation losses study," *Progress In Electromagnetic Research*, Vol. 110, 437–452, 2010.
14. Klemm, M. and G. Troester, "EM energy absorption in the human body tissues due to UWB antennas," *Progress In Electromagnetic Research*, Vol. 62, 261–280, 2006.
15. Kivekas, O., T. Lehtiniemi, and P. Vainikainen, "On the general energy absorption mechanism inthe human tissue," *Microwave and Optical Technology Letters*, Vol. 43, No. 3, 195–201, Nov. 2004.
16. Yan, S. and G. A. E. Vandenbosch, "Radiation pattern reconfigurable wearable antenna based on metamaterial structure," *IEEE Antennas and Wireless Propagation Letters*, Vol. 15, 1715–1718, 2016.
17. Joshi, J. G., S. S. Pattnaik, and S. Devi, "Metamaterial embedded wearable rectangular microstrip patch antenna," *International Journal of Antennas and Propagation*, Vol. 2012, Article ID 974315, 9 pages, 2012.
18. Hu, B., G. P. Gao, L. L. He, X. D. Cong, and J. N. Zhao, "Bending and on-arm effects on a wearable antenna for 2.45 GHz body area network," *IEEE Antennas and Wireless Propagation Letters*, Vol. 15, 378–381, 2016.
19. Balanis, C. A., *Antenna Theory: Analysis and Design*, 3rd Edition, John Wiley & Sons, 2005.
20. FCC: Body tissue dielectric parameters, http://www.fcc.gov/oet/rfsafety/dielectric.html.